The near wake structure of a square cylinder

M. A. Z. Hasan
Mechanical Engineering Department, King Fahd University of Petroleum & Minerals, Dhahran, Saudi Arabia

The near wake structure of a square cross section cylinder in flow perpendicular to its length was investigated experimentally over a Reynolds number (based on cylinder width) range of 6700–43,000. The wake structure and the characteristics of the instability wave, scaling on θ at separation, were strongly dependent on the incidence angle (α) of the freestream velocity. The nondimensional frequency (St_θ) of the instability wave varied within the range predicted for laminar instability frequencies for flat plate wakes, jets and shear layers. For $\alpha=22.5°$, the freestream velocity was accelerated over the side walls and the deflection of the streamlines (from both sides of the cylinder) towards the center line was higher compared to the streamlines for $\alpha=0°$. This caused the vortices from both sides of the cylinder to merge by $x/d\cong 2$, giving the mean velocity distribution typical of a wake profile. For $\alpha=0°$, the vortices shed from both sides of the cylinder did not merge until $x/d\cong 4.5$. The separation boundary layer for all cases was either transitional or turbulent, yet the results showed good qualitative, and for some cases even quantitative, agreement with linearized stability results for small amplitude disturbance waves in laminar separation layers.

Keywords: turbulent and transitional boundary layer; instability wave; self-similarity; initial condition; nonparallel effect and pressure coefficient

Introduction

The formation of vortex streets in cylinder wakes has been a subject of intensive investigations. Rayleigh[1] was first to point out that vortex street formation is related to an instability of the cylinder wake. Later, this was confirmed by Kovasznay[2] via experimental observation. The mechanism of vortex formation and the characteristics of the instability wave associated with the wake have been studied theoretically for simple flows. Stability calculations using measured velocity profiles of the wake far behind a flat plate parallel to uniform flow have been performed by, among others, Sato and Kuriki[3] (temporal instability) and Gaster[4] (spatial instability). Detailed stability calculations for the incompressible wake behind a thin airfoil have been performed by Mattingly and Criminale[5] for both temporal and spatial instability. Triantafyllou *et al.*[6] investigated the nature of the wake instability behind a stationary cylinder, namely whether the wake instability is of the absolute or of the convective type, Bers.[7] The theoretical consideration for these studies is based upon two-dimensional linearized stability theory, and, thus limited to small disturbance waves behind thin bodies or circular cylinders. Comparatively very little attention has been paid to the instability characteristics of large disturbance waves behind bodies of finite dimension and noncircular cross sections.

Interest in the construction of high rise towers and other structures has led to increased emphasis on flow around rectangular, square and other noncircular bodies. The overall time mean and fluctuating drag, lift, and wall pressure for rectangular cross-section cylinders have been investigated by, among others, Lee[8] and Vickery.[9]

The fluctuating pressure on a bluff body surface is due to the velocity fluctuations in the incident stream and to various instabilities in the wake region, such as vortex, shedding, recirculation, and intermittent reattachments (Huot *et al.*[10]). For a square cylinder, the effect of upstream turbulence on the side wall mean pressure and the dependence of the vortex shedding frequency with incident angle of flow has been investigated by Lee,[8] while Rockwell[11] studied the effect of incidence angle on side wall fluctuating pressure. The spectral studies of the pressure field on the upstream face of square cylinder was done by Huot *et al.*[10] Downstream of the separation the fluctuating pressure field is dominated by vortex shedding and has an energetic peak at the shedding frequency. However, studies of the downstream wake and its instability characteristics for flow around noncircular bodies have been rare. Such information is essential, not only to enhance our understanding of the wake structure itself, but also to improve the accuracy of the stability analyses by including the effects of large disturbance and nonparallel flow present for nonstreamlined bluff bodies.

In this paper, the instability wave and the wake structure, immediately behind a square cylinder, have been studied experimentally, including the effect of the incidence angle of the freestream velocity on the wake structure. Also, the results have been compared with the results of Sato and Kuriki[3] and Mattingly and Criminale[5] to identify the validity (if any) and limitations of the linearized stability analysis in predicting flow behind a square cross section cylinder.

Experimental procedure

The experiment was performed in the subsonic wind tunnel in

Address reprint requests to Dr. Hasan at the Mechanical Engineering Department, King Fahd University of Petroleum and Minerals, Dharan 31261, Saudi Arabia.

Received 10 May 1988; accepted 6 February 1989

the aerodynamics laboratory at KFUPM. The cross section of the test section is 1.1 m × 0.8 m, the length being 3 m. The freestream turbulence intensity in the test section was less than 0.1%. A Plexiglas cylinder with square cross section (3.175 cm × 3.175 cm) was used for the experiment. The length of the cylinder was 80 cm, giving a L/d ratio of over 25. This ensured two-dimensional flow in the midspan of the cylinder. This was checked by measuring the mean velocity profiles at two spanwise stations for $x/d=2$. The blockage ratio was less than 3%, and, therefore, no correction was applied to the data. The schematic of the experimental setup is shown in Figure 1(a).

A mechanism at the base of the cylinder was used to set the cylinder at any desired angle of incidence with respect to the freestream velocity. The surface pressure was measured with 0.5 mm pitot holes, five on each side in the midsection of the cylinder. The resolution of the pressure measurement manometer was 0.01 mb.

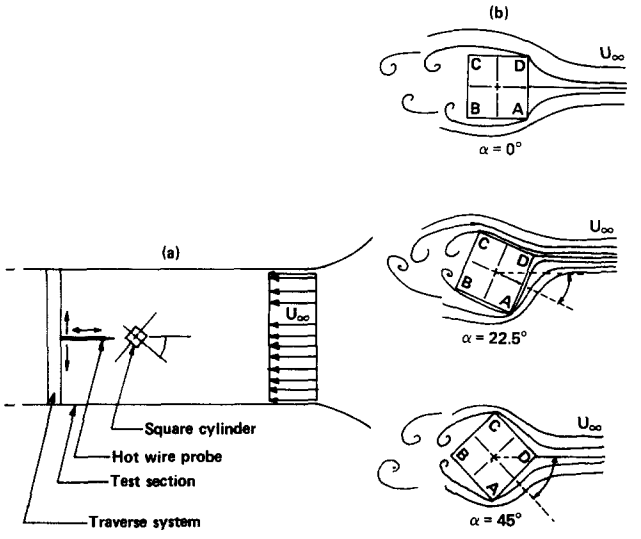

Figure 1(a) The schematics of the experimental setup
Figure 1(b) The qualitative streamlines along the cylinder for various α's

The velocity data were measured with DISA 55M01 hot-wire anemometer system. The anemometer was operated in the constant temperature mode with 50% overheat ratio. The signal was linearized because of the high level of turbulence intensity present in the flow field. The spectral analysis of the velocity signal was performed with a B & K 2033 high resolution signal analyzer with 400 lines. Each data point represents the average of 128 spectra.

A remote controlled traverse system was used to position the probe inside the test section. The resolution of the traverse system is 0.06 mm.

The experimental uncertainty in velocity measurement was found to be less than 1%. The maximum uncertainty in the static pressure measurement was no more than ±5% at the lowest velocity (5.1 m/s) used, while the same dropped below ±1% at the maximum velocity (20.0 m/s) used.

Results and discussion

The Strouhal number

The experiment was performed for four angles of the incident flow over a velocity range of 3.12 m/s to 20.0 m/s. The corresponding Reynolds numbers, Re varied between 6720 and 43,000. The variation of Strouhal number, St with Re is given in Table 1. The shedding frequency of the vortices was measured at $x=2$ cm and $y=0$ cm. It was observed that the shedding frequency was independent of the transverse location of the probe, and, thus the exact location of the probe in y-axis was not critical, except on center plane where the second harmonic of the shedding frequency may have the maximum amplitude. Note that the St values are nearly constant at 0.12 over the entire Reynolds numbers range. The St value corresponding to Re_c (Reynolds number at which flow becomes periodic) for circular cylinder shows an average value of 0.12–0.13 for various experimental studies and time dependent calculations, as listed by Jackson.[12] The St value for a circular cylinder increases with Re increasing from Re_c, and becomes constant at 0.21 (Roshko[13], Cantwell[14]) for $Re>300$. No such increase in St values was observed for the present study. This is due to the fact that the Re values used in the present study were much

Notation

c	$=c_r+c_i$
c_r	Propagation velocity of a disturbance
c_i	Rate of amplification of disturbance
C_p	Pressure coefficient $=P-P_\infty/\frac{1}{2}\rho_\infty U_\infty^2$
d	Width of the cylinder cross section
f	Vortex shedding frequency
H	Shape factor (δ^*/θ)
k	Wave number
L	Length of the cylinder
P	Surface static pressure
P_∞	Freestream static pressure
Re	Reynolds number $(U_\infty d\rho/\mu)$
Re_c	Critical Reynolds number
St	Strouhal number (fd/U_∞)
St_θ	Strouhal number $(f\theta/U_\infty)$
$St_{\theta m}$	Strouhal number $(f\theta/U_{max})$
U	Longitudinal mean velocity
$U_1=V_{dm}$	Maximum velocity defect in the wake
U_2	$=0.0$
U_∞	Freestream velocity in the test section
$U_{\infty x}$	Local freestream velocity at x
U_{max}	Maximum mean velocity at x
u'	Longitudinal fluctuation intensity
u_f	Amplitude of instability wave of frequency f
u_{2f}	Amplitude of instability wave of frequency $2f$
u_{fm}	Maximum amplitude of u_f
V_R	Reference voltage $=3.16\times10^{-9}$ volt
V_d	Velocity defect $(U_\infty-U)$
V_{dm}	Maximum value of V_d
x	Downstream distance
y	Transverse distance
y_b	Half-width of the wake
$y_{0.5}$	Transverse location where $U/U_\infty=0.5$
y_d	$(y-y_{0.5})/\delta^*$
ρ_∞	Freestream density of air
α	Incidence angle of freestream velocity
δ^*	Displacement thickness
θ	Momentum thickness
ζ	$=y/x$
φ	Velocity potential
σ	Similarity parameter for wake behind wedge
erf	Error function

Table 1 The Strouhal numbers for a square cross section cylinder

α (degree)	$Re=(U_\infty d/\nu)\times10^{-3}$	$St=(fd/U_\infty)$	α (degree)	$Re=(U_\infty d/\nu)\times10^{-3}$	$St=(fd/U_\infty)$
0	6.72	0.117	10	10.98	0.136
0	7.77	0.115	10	21.53	0.141
0	9.52	0.122	10	43.06	0.137
0	11.65	0.123	22.5	21.53	0.161
0	14.01	0.124	22.5	43.06	0.166
0	16.73	0.123	45	21.53	0.147
0	19.44	0.123	45	43.06	0.158
0	22.67	0.121	0 (Lee[8])	176	0.121
0	26.07	0.119	15 (Lee[8])	176	0.143
0	28.85	0.121	22.5 (Lee[8])	176	0.129
0	31.82	0.120	45 (Lee[8])	176	0.115
0	35.52	0.122	0 (Vickery[9])	40	0.118
0	38.49	0.121	15 (Vickery[9])	40	0.131
0	41.51	0.120	45 (Vickery[9])	40	0.129
0	43.06	0.120			

higher than the Re_c for a square cylinder. The difference in the St values suggests that the equilibrium St value for a square cylinder is different from that of a circular cylinder. Table 1 also lists St values for other studies with square cylinders and shows excellent agreement with the present data for $\alpha=0°$. Note that the St value increases with increasing α, reaches a maximum at $\alpha=22.5°$ and then decreases with further increase in α. Lee[8] and Vickery[9] observed similar trend in St values with α, except that their numerical values are not the same as ours. The St values for α greater than zero (in Table 1) were calculated based on the projected width of the cylinder perpendicular to the flow direction. It is not clear what length scale was used by Lee[8] and Vickery[9] in their St calculation. The increase in St values with increasing α can be explained by the fact that the flow reattaches at points A and C (Figure 1(b)) for $\alpha=22.5°$ and 45°. This will reduce the wake width compared to the case when flow does not reattach (α less than 22.5°) at points *A* and *C*. The reduced wake width will give reduced longitudinal vortex spacing, if a constant ratio of vortex spacing to wake width is presumed. The reduced longitudinal vortex spacing is equivalent to an increase in the frequency of vortex shedding, and thus to an increase in St values. This also will explain the decrease of St value as α increases from 22.5° to 45°. The validity of the explanation that flow reattaches at points *A* and *C* (Figure 1(b)) can be checked with the mean pressure distribution on the surface of the cylinder.

The mean pressure field

The mean pressure distribution on the surface of the cylinder for four α's and three different freestream velocities is shown in Figure 2. The insets in Figure 2 identify the four surfaces of

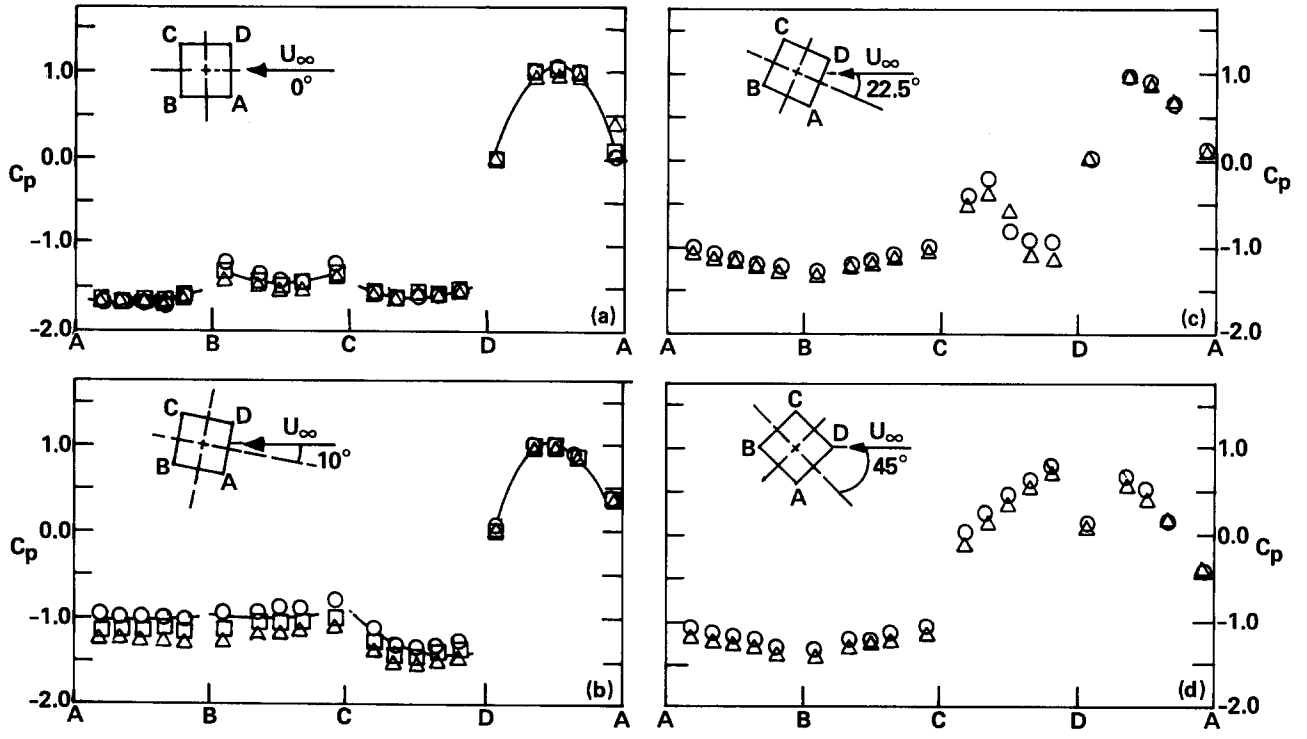

Figure 2 The C_p distribution over the cylinder for various U_∞'s: 0, 5.1 m/s; △, 10.0 m/s; □, 20.0 m/s; ——, Lee[8] *, Huot *et al.*[10] The α values are (a) 0°, (b) 10°, (c) 22.5°, (d) 45°

the cylinder and their relative positions with respect to the freestream velocity. In Figures 2(a)–(b), the solid line represents the data of Lee[8] for uniform flow. Also shown in Figure 2(a) are the data of Huot *et al.*[10] The present data show excellent agreement with the data of Lee[8] and Huot *et al.*[10] In Figures 2(a)–(b), the C_p value is increasing towards point C over the surface CD. This is exactly opposite to the decreasing value of C_p towards point C in Figures 2(c)–(d). A decreasing value of C_p towards point C suggests that the flow reattaches at C and separates beyond C. In Figure 2(a), the C_p values are identical over surfaces AB and CD, and it increases towards the downstream point. This implies that the flow does not reattach at points B and C after being separated at points A and D. This conforms with the explanation provided in the previous subsection regarding the variation of St values with α. The conjectured streamlines corresponding to the data in Figure 2 are also included in Figure 1(b). Note that in Figure 2(b), the C_p value on surface CD shows a sharp increase towards point C. This means the deflection of streamlines from point C towards the centerline is more compared to the corresponding deflection of streamlines from point B, resulting in increased entrainment on side CD. With increasing entrainment, the free shear layer tends to reattach on the sides of the cylinder.

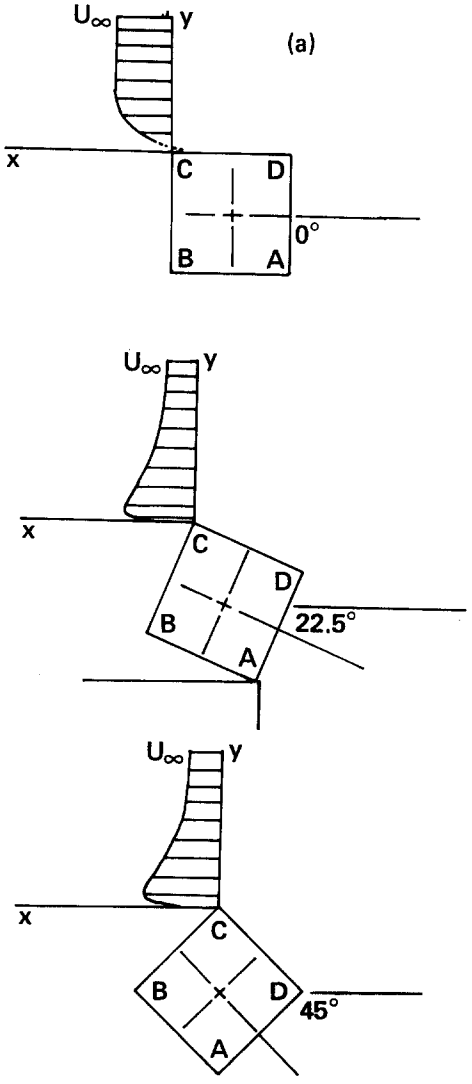

Figure 3(a) The qualitative boundary layer profiles and the coordinate system for the cylinder

The mean and dynamic pressures on the cylinder surface and the instability characteristics downstream of the cylinder are strongly dependent on, among other things, the initial condition, or in this case the condition at separation. The role of the initial condition on the evolution of shear layer instability and the role of outer layer structure on the wall pressure field under a turbulent boundary layer is well established (Hussain and Zedan,[15] Hasan *et al.*[16]). Besides, proper documentation of the initial condition data is necessary for future development of computational models to analyse such flows.

The initial condition

Based on the data of the previous subsections, further investi-

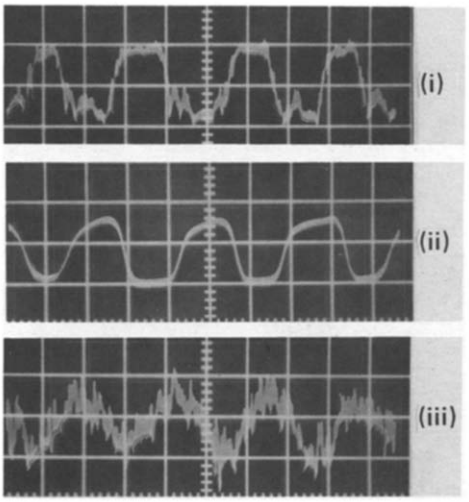

Figure 3(b) The oscilloscope trace for u' in the boundary layer for $U_\infty = 20$ m/s, at $y_{0.75}$. Horizontal scale: 5 ms/div. The α values and vertical scale (volts/div) are (i) 0°, 5.0; (ii) 22.5°–A, 0.5; (iii) 22.5°–B, 2.0

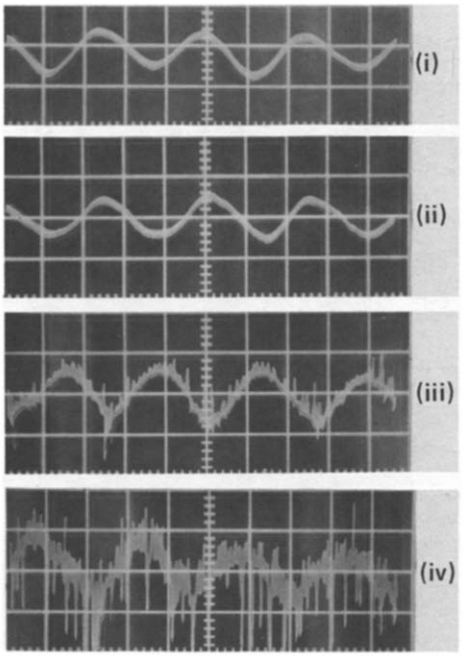

Figure 3(c) The oscilloscope trace for u' in the boundary layer for various locations for $\alpha = 22.5°$ and $U_\infty = 5.1$ m/s. Horizontal and vertical scales are the same for all cases. The y location and edge of the cylinder are (i) $y_{0.45}$, A; (ii) $y_{0.95}$, C; (iii) $y_{0.85}$, C; (iv) $y_{0.70}$, C

gation of the boundary layer characteristics at separation and the downstream evolution of the instability wave was carried out for $U_\infty = 5.1$ m/s and 20.0 m/s for $\alpha = 0.0°$, 22.5°, and 45°.

The schematics of the boundary layer profiles and the coordinate system for various α's are shown in Figure 3(a). Due to symmetric configurations, data were taken on one side of the cylinder for $\alpha = 0°$ and 45°. For $\alpha = 22.5°$, data were taken on both sides of the cylinder, since flow at point A (Figure 1(b)) was found to be quite different from flow at point C. For $\alpha = 0°$, the edge C instead of edge D (Figure 3(a)) of the cylinder was used to document the initial condition for the convenience of positioning the probe with minimum interference with the flow. The velocity profile was measured at 1 mm downstream of the respective cylinder corners.

Figure 3(b) shows the oscilloscope traces of the velocity signal in the boundary layer at transverse location $y_{0.75}$, where $U/U_{\infty x} = 0.75$, for $\alpha = 0°$ and 22.5° at $U_\infty = 20$ m/s. Note that the vertical scales are different for the three traces. While the frequency of the periodic signal remains nearly constant for all three cases, the amplitude of the periodic signal is maximum for $\alpha = 0°$, followed by the amplitude for $\alpha = 22.5° - C$ and $22.5° - A$. The velocity signal at edge A for $\alpha = 22.5°$ is completely laminar. This is not the case at the other edge (edge C), where a significant unsteadiness is present in the signal. For $\alpha = 0°$, the velocity signal shows minor unsteadiness superimposed on the laminar periodicity.

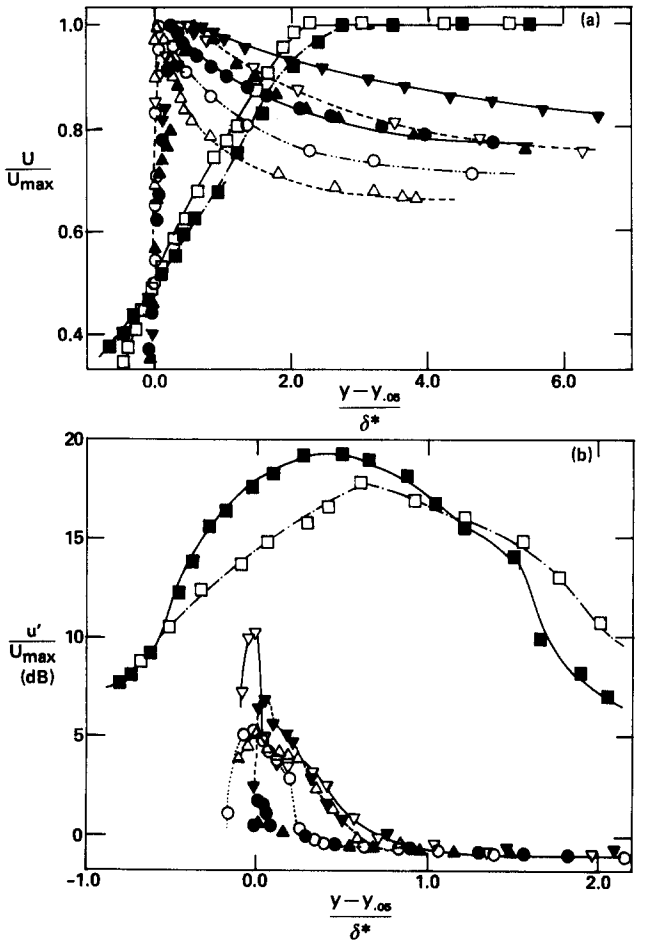

Figure 4 Longitudinal mean velocity (a) and turbulence intensity (b) distribution in the boundary layer for $U_\infty = 5.1$ m/s (open symbols) and 20.0 m/s (solid symbols). The angle of incidence (α) and edge of the cylinder are □, $0° - C$; △, $22.5° - A$; ▽, $22.5° - C$; ○, $45° - C$

The difference in the boundary layer signals between edges A and C for $\alpha = 22.5°$ led us to investigate the nature of the entire boundary layer profile. Figure 3(c) shows the oscilloscope traces at various transverse locations for $U_\infty = 5.1$ m/s. The periodic signal representing the shedding frequency remained laminar throughout the entire boundary layer profile at edge A. At edge C, the periodic signal was laminar only in the outer part of the boundary layer (Figure 3(c-ii)), and the unsteadiness appeared at $y_{0.85}$ (where $U/U_{\infty x} = 0.85$). This unsteadiness can be explained by the surface pressure data in Figure 2(c). The flow on side DC first decelerates followed by sudden acceleration, causing the streamline to bend and reattach at point C. This reattachment process is very unsteady, especially close to the wall. Contrary to this, the flow on sides DA and AB only accelerates, causing the flow to remain attached on these walls.

Figures 4(a)–(b) show the longitudinal mean velocity U and turbulence intensity u' distribution in the boundary layer for $U_\infty = 5.1$ m/s and 20.0 m/s. The open and solid symbols represent the data for $U_\infty = 5.1$ m/s and 20.0 m/s, respectively. Unless otherwise specified, the lines connecting the data points are for visual aid only. In Figure 4(a), the vertical axis is U/U_{max}, where U_{max} is the maximum longitudinal velocity in the boundary layer. Traditionally, in boundary layer calculations, the mean velocity is normalized with freestream mean velocity U_∞. For the present study, the freestream velocity accelerates significantly over the side surfaces of the cylinder when $\alpha > 0$. Note that at 5.1 m/s, the freestream velocity U_∞ at edge A is only about 70% of the maximum velocity in the boundary layer for $\alpha = 22.5°$. The maximum acceleration of the freestream velocity takes place at edge A for $\alpha = 22.5°$, followed by $\alpha = 45°$ and at edge B for $\alpha = 22.5°$. No such acceleration of the freestream velocity takes place for $\alpha = 0°$. The acceleration of the freestream velocity along the side wall of the cylinder is consistent with the wall pressure distributions shown in Figures 2(a)–(d). For $\alpha = 0°$, the boundary layer data acquisition was terminated when $U/U_{max} < 0.25$. As the probe moved towards the wall beyond this point, the mean velocity decreased very slowly and sometimes even increased, suggesting the presence of separation and reversed flow. The boundary layer parameters, i.e., displacement thickness δ^* and momentum thickness θ were calculated with the following expressions:

$$\delta^* = \int_{y_{0.25}}^{\infty} \left(1 - \frac{U}{U_{max}}\right) dy$$

$$\theta = \int_{y_{0.25}}^{\infty} \frac{U}{U_{max}} \left(1 - \frac{U}{U_{max}}\right) dy$$

Due to separation and reversed flow for $\alpha = 0°$, significant errors can occur in the calculation of wall location by extending the velocity profile. Thus, no attempt was made to extend the above integrations to $y_{0.0}$ (where $U/U_{\infty x} = 0.0$). This is why the x coordinate in Figure 4 is given in $y_d\,(= (y - y_{0.5})/\delta^*)$. The maximum error in the calculation of δ^* and θ, using the above expressions, was estimated to be less than 2% except for $\alpha = 0°$. The shape factor (H) values listed in Table 2 suggest that the boundary layer is transitional for $\alpha = 0°$, while for other cases, the boundary layer is turbulent. In Figure 4(a), the U_{max} location moves away from the wall for $\alpha = 22.5° - C$ ($y_d \approx 1$) compared to $\alpha = 45°$ and $22.5° - A$ ($y_d \approx 0$). This shift in the location of U_{max} is due to the higher acceleration at edge A compared to edge C for $\alpha = 22.5°$.

Figure 4(b) shows the longitudinal turbulence intensity distribution in the boundary layer for the data in Figure 4(a). The y-coordinate is in arbitrary scale, but the relative values for various cases are accurate. The maximum turbulence intensity in the boundary layer is significantly higher for $\alpha = 0°$ cases compared to the other cases. This is consistent with the

Table 2 Boundary layer parameters

U_∞ (m/s)	α (degree)	δ^* (mm)	θ (mm)	$H=\delta^*/\theta$	St_θ	$St_{\theta m}$
5	0	4.8079	2.5091	1.9162	0.0098	0.0098
5	22.5–*A**	10.5894	7.5364	1.405	—	—
5	22.5–*C**	8.7879	7.0466	1.247	0.0272	0.0203
5	45	7.7826	5.888	1.3217	0.01933	0.0137
20	0	3.9646	2.0046	1.9778	0.00753	0.00753
20	22.5–*A**	4.588	3.4928	1.3135	0.01397	0.0105
20	22.5–*C**	5.7624	4.7729	1.2057	0.0194	0.0156
20	45	4.6851	3.8706	1.21	0.0136	0.0105

* Represents edge of the cylinder (see Figure 1(b))

oscilloscope traces in Figure 3(a). The fluctuating wall pressure is directly related to the turbulence intensity level in the outer part of the boundary layer. Thus, the wind loading on a square cross section structure can be reduced dramatically by arranging the incident flow to be angled to the sides of the structure.

Downstream evolution of the wake instability wave

The flow behind a circular cylinder has been found to be quite complicated. The flow behind a square cylinder is even more complex. Thus, a major part of the theoretical studies (Sato and Kuriki,[3] Mattingly and Criminale,[5] Michalke[17]) deals with small disturbances in shear layers, and neglects the nonparallel effects. The axial evolution of the longitudinal fluctuation intensity (u_f) of the instability wave of frequency f was documented along a constant transverse location ($y=0$ cm in Figure 3(a)) to shed light on the instability characteristics of large amplitude disturbance waves with large deflection of the shear layer streamlines.

Figures 5(a)–(c) show the variation of u_f in the downstream direction for three α's at two different U_∞'s, i.e., 5.1 m/s and 20 m/s. For $\alpha=0°$ (Figure 5(a)), the amplitude of the wake instability wave u_f grows exponentially in the downstream direction up to $x=1.0$–1.5 cm. The linear part of the curve in Figures 5(a)–(c) represents the region where amplitude of the instability wave grows exponentially. For $\alpha=22.5°$ and 45.0° (Figures 5(b)–(c)), the amplitude of u_f drops sharply between $x=0.5$ cm and 1.0 cm, followed by a linear region. The dotted lines in Figures 5(a)–(c) show the deviation from the linear region. Note that the drop in the amplitude of u_f between $x=0.5$ cm and 1.0 cm for $\alpha=22.5°$ (Figure 5(b)) is more along edge A than edge C. The behavior of u_f along edge C for $\alpha=22.5°$ lies between that along $\alpha=0°$ and 45°. The sudden drop in the amplitude of u_f was also observed for the instability

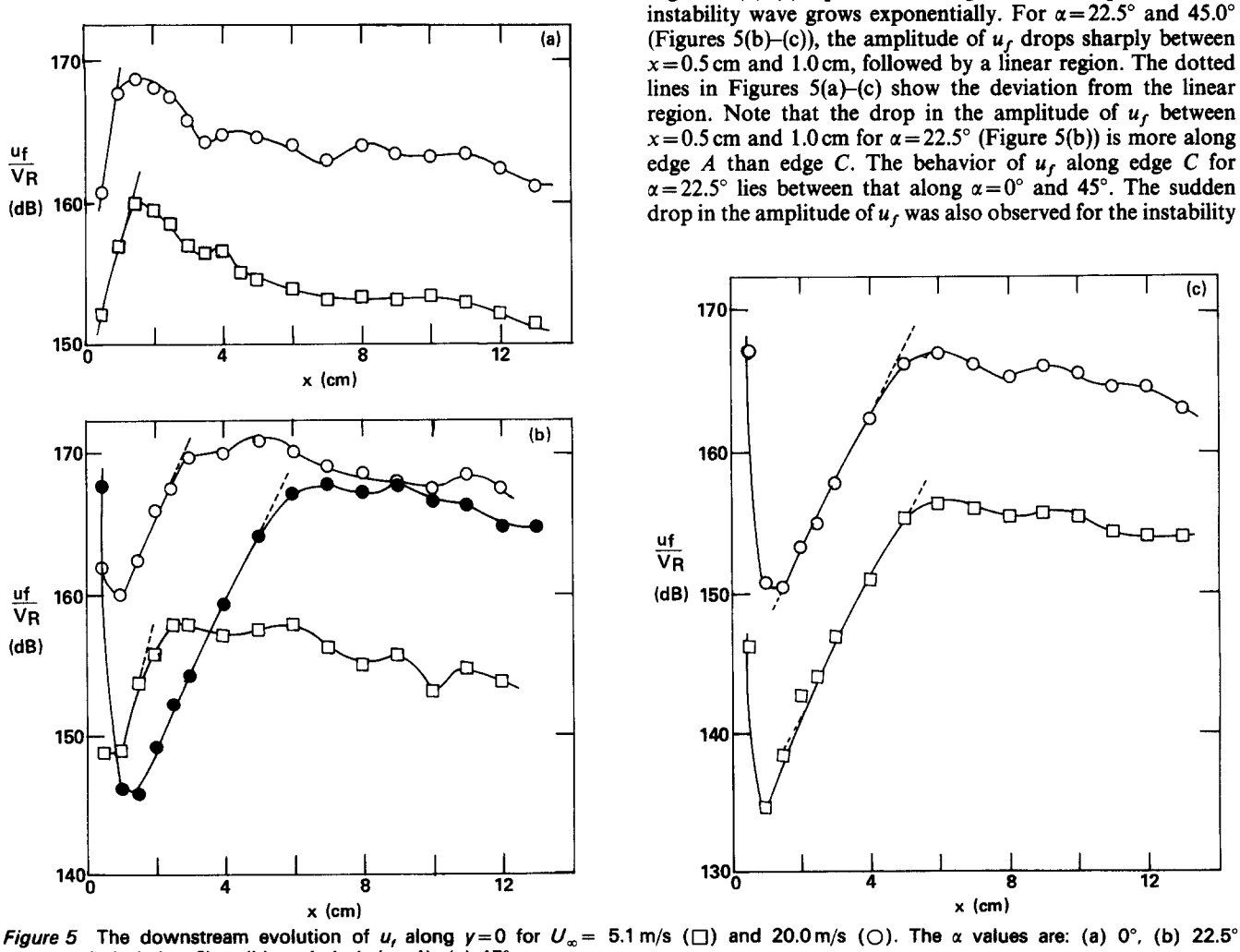

Figure 5 The downstream evolution of u_f along $y=0$ for $U_\infty=$ 5.1 m/s (□) and 20.0 m/s (○). The α values are: (a) 0°, (b) 22.5° open symbols (edge C), solid symbols (edge A), (c) 45°

wave in a whistler nozzle (Hasan and Hussain[18]). The interaction between a hydrodynamic instability wave and an acoustic wave can cause a sudden drop in u_f. Unlike the whistler nozzle, no such coupling between hydrodynamic and acoustic waves is present for the data in Figure 5. The sharp drop in the instability wave amplitude may be associated with the sudden expansion of the flow in the presence of a side wall. The exact mechanism by which the drop in u_f occurs and its dependence on the distance between separation point and the side wall remains to be explored.

In Figures 5(a)–(c), the amplitude of the instability wave is expressed in dB with respect to a reference voltage, $V_R = 3.16 \times 10^{-9}$ volt. For $\alpha = 0°$, the u_f is maximum at $x = 1.0$–1.5 cm, the corresponding value for $\alpha = 45°$ is about 5.5 cm. For all cases the linear region is followed by a nonlinear region.

Figure 6(a) shows the data for few cases from Figure 5, except that the amplitude is normalized with the mean velocity at $x = 0.5$ cm and $y = 0.0$ cm, and the x-coordinate is normalized with the momentum thickness θ at separation. The corresponding amplitudes of the second harmonic ($2f$) are shown in Figure 6(b). The arrows in Figure 6(a) identify the location where the $2f$ component first appears in the u'-spectra. Note that in Figure 6(a), the amplitudes for various cases lie in a narrow range compared to Figures 5(a)–(c). The u_f is maximum for $\alpha = 0°$ and $U_\infty = 20$ m/s, which is consistent with the maximum turbulence intensity in the boundary layer at separation (Figure 4(a)). The maximum amplitude for the instability wave is higher

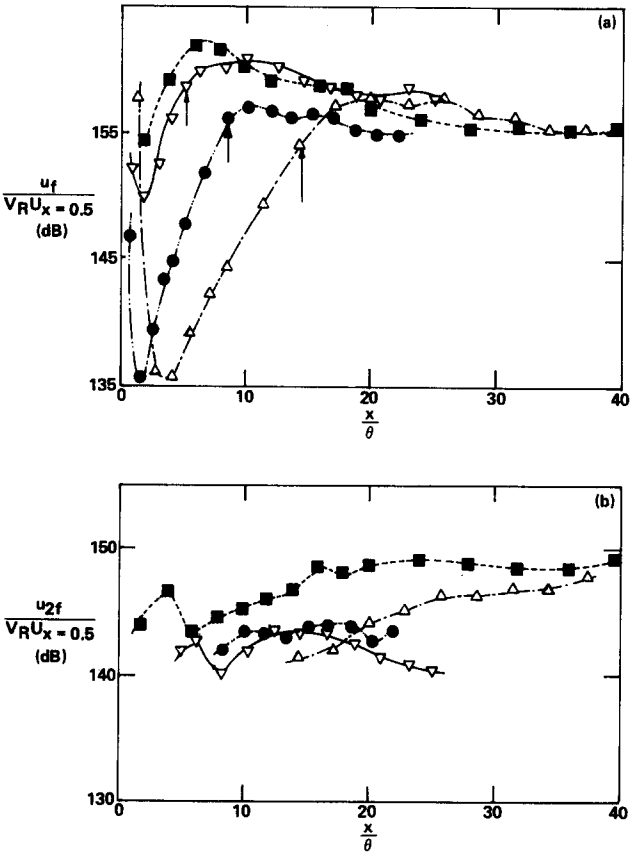

Figure 6 The downstream evolution of (a) u_f and (b) u_{2f} along $y = 0$ for $U_\infty = 5.1$ m/s (solid symbols) and 20.0 m/s (open symbols). The amplitude is normalized with mean velocity at $x = 0.5$ cm. The α and cylinder edge are □, 0°–*C*; △, 22.5°–*A*; ▽, 22.5°–*C*; ○, 45°–*C*

for transitional boundary layer than turbulent boundary layer at separation. A similar trend for the instability wave amplitude with respect to the initial condition at separation was observed by Hasan and Hussain[18] for a whistler nozzle with an axisymmetric boundary layer. The peaks of the u_f distribution in Figure 6(a) fall between $x/\theta = 6$–20. For laminar separation, the peak of the instability wave for free shear flows occurs at $x/\theta = 60$–100 (Husain and Hussain[19]).

In Figure 6(a), the location at which the second harmonic ($2f$) component appears, coincides with the location where the amplification of u_f deviates from being exponential except for $\alpha = 0°$. A similar observation was made by Sato and Kuriki[3] in their study of transition in the wake of a thin plate. They attributed the deviation from linear region and the appearance of higher harmonics to transition from laminar to turbulent flow. It is interesting that in the present study a linear region (where the instability wave grows exponentially) is present even when the boundary layer at separation is not laminar. The similar behavior of the present data for u_f with Sato and Kuriki's led us to compare our results with the theoretical analyses of Sato and Kuriki[3] and Mattingly and Criminale[5] based upon two-dimensional linearized stability theory.

In studying the linearized stability problem for an inviscid fluid, it is assumed that the disturbance velocity is small compared to the laminar time averaged flow field and the flow field is locally parallel. This last assumption is the most restrictive one for wake flow, requiring in essence that at each station behind the cylinder the properties of the wake are adequately represented, locally, by the stability properties of a parallel flow having the same average velocity profile. Large fluctuation intensity and nonparallel effect present for flow behind the square cylinder may raise questions about the appropriateness of comparing our data with the results of linearized stability analyses. It should be pointed out that the current state of knowledge of the nonlinear stability of parallel flows is much less complete than that of Bernard convection or Couette flow. Further, nearly parallel flow brings complication into the theory (Drazin and Reid[20]). The combined effects of nonlinearity and divergence of basic flow have yet to be treated satisfactorily even for Blausius boundary layer. No similar studies for wake flows are available in the literature to the best of our knowledge. Thus, it was considered appropriate to compare our results with the results of Sato and Kuriki[3] and Mattingly and Criminale.[5] In these studies, the "inviscid" form of the well known Orr-Sommerfeld equation,

$$\left(\frac{U}{U_\infty} - c\right)(\varphi'' - k^2\varphi) - \frac{U''}{U_\infty}\varphi = 0$$

was solved with the following boundary conditions:

$$\varphi(0) = 1 \quad \varphi'(0) = 0 \quad \varphi'(\pm\infty) + k\varphi(\pm\infty) = 0$$

An analytical expression for the mean velocity distribution based on the measured profile was substituted in the governing equation, and—through numerical integration—a set of eigenvalues satisfying the boundary conditions was obtained.

The average value of the nondimensional frequency kc_r ($= 2\pi f b/U_\infty$) of the most highly amplified wave was 0.62 from Sato and Kuriki's[3] studies. The corresponding values for kc_r for the present study are: 0.62 ($\alpha = 22.5°$, $x = 6$ cm), 0.76 ($\alpha = 22.5°$, $x = 13$ cm) and 0.90 ($\alpha = 0°$, $x = 13$ cm).

The theoretical value for kc_r for neutral instability at infinite Re is 0.92. Thus, the shedding frequency for the square cylinder is found to lie inside the unstable zone of the theoretical stability diagram for a flat plate wake.

Another measure of the natural instability frequency for a shear layer is the Strouhal number (St_θ) based on momentum thickness θ at separation. Investigations in both axisymmetric

and plane laminar shear layers in a number of independent facilities by Husain and Hussain[19] reveal that St_θ for naturally occurring wave falls in the range 0.0125–0.0155. The St_θ values reported by other investigators (see Ref. 19) varied over a range of 0.006–0.016. The St_θ values for the data shown in Figure 6(a) are listed in Table 2, and vary in the range 0.007–0.027. When the Strouhal number was calculated based on maximum velocity $U_{max}(St_{\theta max})$ and not the freestream velocity U_∞, the Strouhal numbers varied in the range 0.007–0.020. Note that the Strouhal number based on the shedding frequency of the square cylinder is within the natural instability frequency range for laminar shear layers, although the boundary layer for the square cylinder at separation is either transitional or turbulent. This suggests that the nondimensional instability frequency scaled with θ is independent of the initial condition at separation. The maximum velocity at separation, and not the freestream velocity, appears to be the appropriate velocity scale for estimating the nondimensional instability frequency for flows undergoing acceleration in the boundary layer at the separation point. St_θ value lower or higher than 0.011 (when maximum amplification of the instability wave occurs) can be attributed to the coupling between the shear layer instability mode and the instability of the whole flow dictated by the width of the cylinder perpendicular to the freestream velocity.

Results obtained from the linearized stability theory (Sato and Kuriki[3]) are capable of predicting the general characteristics of the instability wave for a square cylinder with large amplitude disturbance. The discrepancy in the kc_r values between our data and Sato and Kuriki's[3] analysis could be due to the following factors: large fluctuation amplitude at separation, local acceleration of the mean velocity and nonparallel effects, among others, present for the flow over a square cylinder.

The accuracy of the stability analysis for bluff bodies with large amplitude disturbance at separation can be improved by including the effects of the above mentioned factors in the theoretical analysis. This calls for more detailed investigation of the near wake structure itself. In an attempt to increase our understanding about the wake structure, measurement of the mean velocity, fluctuation amplitude, and instability wave amplitude were carried out across the wake.

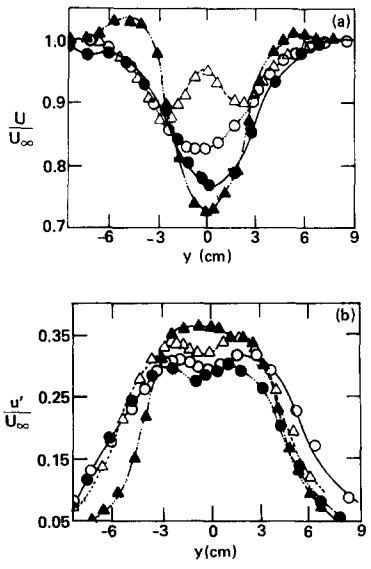

Figure 7 Distribution of normalized (a) U/U_∞ and (b) u'/U_∞ for $\alpha=0°$ (open symbols) and 22.5° (solid symbols) in the wake for $U_\infty=20.0$ m/s. The downstream locations (x) are △, 6 cm; ○, 13 cm

The wake structure

The longitudinal mean velocity and turbulence intensity profiles for the wake at two downstream locations, i.e., $x=6$ cm and 13 cm at $U_\infty=20$ m/s are shown in Figures 7(a)–(b). The open and solid symbols represent $\alpha=0°$ and 22.5° respectively. For $\alpha=0°$, the velocity profile has two minima for $x=6$ cm (Figure 7(a)) compared to one minimum for the other three cases. The two minima in the mean velocity profile will be present if the vortices shed from both sides of the cylinder do not merge. Note that for $\alpha=0°$, the outer part of the wake profile collapses for both $x=6$ and 13 cm. This indicates that the wake did not grow in the direction away from the cylinder between $x=6$ cm and 13 cm. For $\alpha=22.5°$ (solid symbols), the vortices from both edges of the cylinder merge by $x=6$ cm. Similar to $\alpha=0°$ case, the wake does not grow in the outer direction for $\alpha=22.5°$, but the velocity distribution within the wake changes between $x=6$ cm and $x=13$ cm. The velocity defect at the center of the wake is lower at $x=13$ cm than at $x=6$ cm. Usually the velocity defect at the wake center decreases at the expense of the growth of the wake in the outward direction. In Figure 7(a), for $\alpha=22.5°$, note that the mean velocity in the outer part of the wake exceeds the freestream velocity at $x=6$ cm. With downstream distance, the velocity in the outer part of the wake decreases below the freestream velocity, and thus reduces the centerline defect without growing in the outward direction.

The velocity in the outer part of the wake exceeding the freestream velocity was also observed by Sato and Kuriki.[3] They explained this phenomenon wih a model that assumes double row of vortices developing through the transverse displacement of a single row of vortices that originally lie along the wake center-plane. A different mechanism in contrast to that of Sato and Kuriki[3] was proposed by Mattingly and Criminale[5] to explain high velocity in the outer part of the wake. They argued that the superposition of the disturbance vorticity upon that of the mean flow gives rise to vorticity concentrations located off the wake center-plane. The conclusion was drawn that the classic von Karman vortex street formed behind streamlined bodies has its origin in the near wake region. In Figure 7(a), the high velocity in the outer part of the wake at $x=6$ cm and $\alpha=22.5°$ is due to the initial condition at separation, in particular the surface pressure distribution, and consequently the velocity profile in the boundary layer. For $\alpha=22.5°$, the mean velocity in the outer part of the boundary layer is accelerated (Figure 4(a)) with respect to the freestream velocity due to pressure drop on surface DA and DC (Figure 2(c)). This acceleration of the mean velocity in outer part of the boundary layer persists even in the wake velocity at $x=6$ cm. This argument is further strengthened by the fact that the amount by which the mean velocity exceeds the freestream velocity at $x=6$ cm is not equal on both sides of the wake and is proportional to the acceleration of the mean velocity at the initial boundary layer. As the wake travels further downstream, the outer part of the vortices slows down while the inner part accelerates. This will explain the velocity profile shown in Figure 7(a).

Figure 7(b) shows the longitudinal turbulence intensity (u') distribution across the wake corresponding to the mean velocity distribution in Figure 7(a). The maximum turbulence intensity occurring slightly off the center of the wake, is about 35% of the mean velocity. This is significantly higher than the value (about 5%) reported by Sato and Kuriki[3] for the wake behind a thin flat plate or that in the self-preservation region of small deficit wake (Wygnanski *et al.*[21]). This fact might be explained by the disturbance at the trailing edge of flat plate or airfoil being much smaller than the disturbance in the trailing edge boundary layer of a square cylinder. Note that the u' profiles have two peaks with a local minimum between the peaks. This

minimum represents the wake center. For $\alpha=22.5°$, the location of this local minimum shifts from $y\approx -1$ cm to $y\approx -1.5$ cm as the wake travels from $x=6$ cm to 13 cm. The shift of the local minimum for u' suggests that the vortex shed from edge A (Figure 2(c)) has moved to the other side of the centerline. The local minimum for u' does not shift from the center line for $\alpha=0°$. The u' distribution gives a global picture of the overall turbulence intensity in the wake. In an attempt to gain further insight into the characteristics of the wake instability, the transverse distribution of the instability wave amplitude (u_f) and its second harmonic (u_{2f}) were measured.

The transverse distribution of u_f and u_{2f} is shown in Figures 8(a)–(b) for $\alpha=22.5°$ and $\alpha=0°$, respectively. The open and solid symbols represent u_f and u_{2f} components respectively. For both $\alpha=0°$ and 22.5°, the u_f shows peak at $y\approx\pm 2$ cm. At the center of the wake ($y=0$), the u_f drops sharply, while u_{2f} reaches its maximum value. The vortices shed alternately from the two sides of the cylinder and moving towards the center plane of the wake will give such a distribution for u_f and u_{2f}. This is consistent with the measurement and theoretical calculations of Mattingly and Criminale[5] and Sato and Kuriki.[3] The distribution of u_f shown in Figure 8 is qualitatively similar to the distribution obtained theoretically for the symmetrical mode of disturbance in the wake of a thin plate. This suggests that the most amplified disturbance mode for a large width square cylinder is symmetrical. It should be pointed out that in Figure 8(b), the distribution of u_{2f} is shown only for $x=13$ cm. No u_{2f} component was observed in the velocity spectra at $x=6$ cm for $\alpha=0°$. This confirms our explanation for the mean velocity profile in Figure 7(a), that for $\alpha=0°$, the vortices from both sides of the cylinder do not merge sufficiently at $x=6$ cm to produce detectable second harmonic signals.

In a recent study of the near-wake of an axisymmetric semi-elliptical afterbody, Merz *et al.*[22] showed that the wake mean velocity profile became self-similar by one length scale in the downstream direction when the velocity data were plotted using a V_d/V_{dm} coordinate, contrary to the prior evidence that self-similarity takes place for $x/d=40$ or more (see Wygnanski *et al.*[21]).

The mean velocity data of Figure 7(a) are shown using the V_d/V_{dm} coordinate in Figure 9(a), to determine whether the wake profiles show self-similarity in the near field like the flow

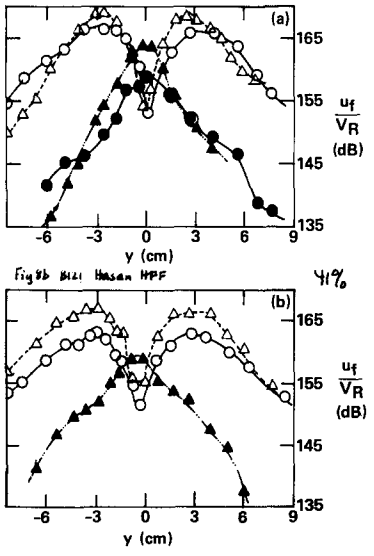

Figure 8 Distribution of u_f (open symbols) and u_{2f} (solid symbols) in the wake for $U_\infty=20.0$ m/s. (a) $\alpha=22.5°$ (b) $\alpha=0°$. The symbols are △, $x=6$ cm; ○, $x=13$ cm

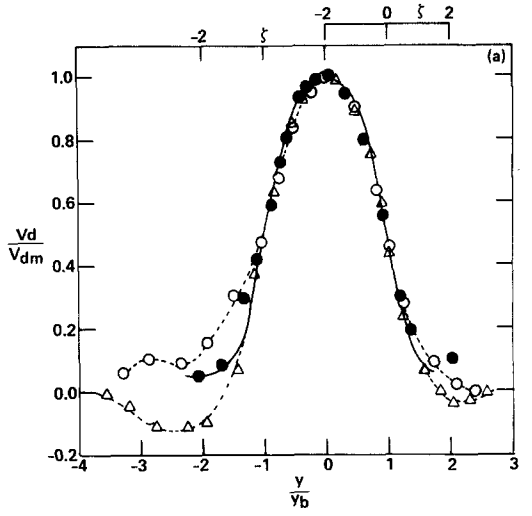

Figure 9(a) The data of Figure 7(a) in V_d/V_{dm} versus y/y_b (and ζ) coordinate for $\alpha=0°$ (solid symbols) and $\alpha=22.5°$ (open symbols). △, $x=6$ cm; ○, $x=13$ cm; ———, Tanner's equation (Ref. 23)

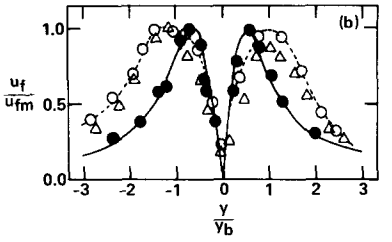

Figure 9(b) The distribution of u_f/u_{fm} for $\alpha=0°$ (solid symbols) and 22.5° (open symbols) at $U_\infty=20.0$ m/s. For symbols see Figure 9(a). ———, (Ref. 5)

behind semielliptic afterbody (Merz *et al.*[22]). The data at $x=6$ cm and for $\alpha=0°$ are not shown in Figure 9(a). Using velocity defect coordinates, the mean velocity profiles collapse only in the inner part of the wake, and do not show self-similarity. For $\alpha=22.5°$, the half-width of the wake was calculated separately on each side of the wake. Note that the asymmetric nature of the wake for $\alpha=22.5°$ is clear in Figure 9(a). The solid line in Figure 9(a) represents the following equation proposed by Tanner (see Schlichting[23]) for wakes behind bluff bodies:

$$U=\frac{U_1+U_2}{2}\left\{1+\frac{U_1-U_2}{U_1+U_2}\,\mathrm{erf}\,\xi\right\}$$

where $\zeta=y/x$, $U_1=$maximum velocity defect, and $U_2=0$.

The agreement between the equation and the measured wake profile is very good for $\alpha=0°$. The equation fails to predict the measured data when the wake is not symmetric about the center line ($\alpha=22.5°$), and particularly for large values of x.

As the u_f distribution for the square cylinder showed qualitative similarity with the distribution obtained theoretically for the symmetrical mode of disturbance in a small wake, a comparison of the data was made with Mattingly and Criminale's[5] result for quantitative agreement. The u_f data of Figure 8 are shown in Figure 9(b) using u_f/u_{fm} versus y/y_b coordinates. The solid line in Figure 9(b) represents the linearized stability analysis result of Mattingly and Criminale.[5] Note that the data for $\alpha=0°$ show excellent agreement with the solid line, while for $\alpha=22.5°$ the agreement is fairly good in the inner part of the wake only. It appears that the characteristics of the

instability wave for asymmetric large disturbance may be predicted by linearized stability analysis, provided an appropriate analytic expression describing the mean velocity profile in the wake is used in the governing equation.

Conclusions

The experimental investigation of the flow past a square cylinder, with varying incidence angle of the freestream flow sheds new light about the wake structure and the instability waves associated with the wake.

The variation in the incidence angle (α) of the freestream velocity changed the pressure distribution on the cylinder surface, and thus the boundary layer characteristics (i.e., the initial condition) at the separation points. The peak turbulence intensity in the boundary layer was maximum for $\alpha=0°$, and was significantly higher compared to other values for α, with the minimum occurring for α between 0° and 45°. The boundary layer at separation was turbulent for $\alpha=22.5°$ and 45°, while it was transitional for $\alpha=0°$.

Although the separation boundary layer was either transitional or turbulent for all cases, the amplitude of the wake instability wave showed a linear region (where the wave amplitude grows exponentially) followed by the nonlinear region, similar to the instability wave growth in laminar wake or shear flows and the nondimensional frequency St_θ for the square cylinder varied within the range (0.006–0.020) of laminar instability frequency.

For $\alpha=0°$, the vortices shed from two sides of the cylinder did not grow until the point $x=13$ cm. For $\alpha=22.5°$, the vortices from each side of the cylinder moved towards the centerline and merged by $x=6$ cm, thus giving a second harmonic component in the velocity spectra. This rapid merging of the vortices towards the centerline was due to the accelerating boundary layer at separation for $\alpha=22.5°$.

The distribution of the instability wave amplitude across the wake showed excellent quantitative agreement (for $\alpha=0°$) with the linearized stability analysis for the wake behind a thin airfoil (Mattingly and Criminale[5]). For $\alpha=22.5°$, the u_f distribution showed only qualitative agreement with the theoretical analysis and this disagreement was attributed primarily to nonparallel effects present in the flow around the square cylinder. The above results confirm that in the linearized stability analyses, the assumption of locally parallel flow is more restrictive than the assumption of small perturbation velocity. The data presented will serve as quantitative basis for the future development of theoretical models addressing the nonparallel effect and high unsteadiness at separation.

Acknowledgments

The author would like to acknowledge the college of graduate research at KFUPM for supporting this work. The author is grateful to Professor A. K. Kar for the use of B & K analyzer and to Mr. John Corner for ME machine shop for helping with the models. Also, thanks are due to Professor M. U. Budair for many illuminating discussions on this topic and to Professor H. I. Abualhamayel for reviewing the manuscript.

References

1 Rayleigh, L. *Theory of Sound*, vol. 2, Dover, 1945
2 Kovasznay, L. S. G. *Proc. R. Soc. A, Lond.* 1945, **198**, 174–190
3 Sato, H. and Kuriki, K. *J. Fluid Mech.*, 1961, **11**, 321–352
4 Gaster, M. *Prog. Aero. Sci.* 1965, **6**, 251–270
5 Mattingly, G. E. and Criminale, W. O. *J. Fluid Mech.*, 1972, **51**, 233–272
6 Triantafyllou, G. S., Triantafyllou, M. S., and Chryssostomidis, C. *J. Fluid Mech.*, 1986, **170**, 461–477
7 Bers, A. Basic plasma physics I. In *Handbook of Plasma Physics*, ed. M. N. Rosenbluth and R. Z. Sagdeev, vol. 1, chap. 3.2, North-Holland, 1983
8 Lee, B. F. *J. Fluid Mech.*, 1975, **69**, 263–282
9 Vickery, F. J. *J. Fluid Mech.*, 1966, **25**, 481–494
10 Huot, J. P., Roy, C., and Arbey, H. *J. Fluid Mech.*, 1986, **162**, 283–298
11 Rockwell, D. O. *J. Fluids Engg., Trans. ASME*, September 1977, 511–516
12 Jackson, C. P. *J. Fluid Mech.*, 1987, **182**, 23–45
13 Roshko, A. *J. Fluid Mech.*, 1961, **10**, 345–356
14 Cantwell, B. J. A flying hot-wire study of the turbulent near wake of a circular cylinder at a Reynolds number of 140000. Ph.D. thesis, California Institute of Technology, Pasadena, California, 1976
15 Hussain, A. K. M. F. and Zedan, M. F. *The Physics of Fluids*, 1978, **21**, 1100–1112
16 Hasan, M. A. Z., Casarella, M. J., and Rood, E. *Shear Flow-Structure Interaction Phenomenon, ASME*, 1985, **1**, 89–95
17 Michalke, A. *J. Fluid Mech.*, 1965, **23**, 521–544
18 Hasan, M. A. Z. and Hussain, A. K. M. F. *J. Fluid Mech.*, 1982, **115**, 59–89
19 Husain, Z. D. and Hussain, A. K. M. F. *AIAA J.*, 1983, **21**, 1512–1517
20 Drazin, P. G. and Reid, W. H. *Hydrodynamic Stability*, Cambridge University Press, 1982
21 Wygnanski, I., Champagne, F., and Marasli, B. *J. Fluid Mech.*, 1986, **168**, 31–71
22 Merz, R. A., Yi, C. H., and Przirembel, C. E. G. *AIAA J.*, 1985, **23**, 1512–1517
23 Schlichting, H. *Boundary Layer Theory*, 7th ed., McGraw-Hill, New York, 1979